The 5th Joint International Conference on Multibody System Dynamics
June 24 –28, 2018, Lisbon, Portugal

A new simplified approach to deal with conformal contact in railway dynamics

Filipe Marques[1], Hugo Magalhães[2], Binbin Liu[3], João Pombo[2,4], Paulo Flores[1], Jorge Ambrósio[2] and Stefano Bruni[3]

[1] *MIT-Portugal Program, CMEMS-UMinho, Departamento de Engenharia Mecânica, Universidade do Minho, Campus de Azurém, 4804-533 Guimarães, Portugal, {fmarques,pflores}@dem.uminho.pt*
[2] *LAETA, IDMEC, Instituto Superior Técnico, Universidade de Lisboa, Avenida Rovisco Pais 1, 1049-001 Lisboa, Portugal, {hugomagalhaes,jorge.ambrosio}@tecnico.ulisboa.pt*
[3] *Dipartimento di Meccanica, Politecnico di Milano, Via La Masa 1, Milano 20156, Italy, {binbin.liu,stefano.bruni}@polimi.it*
[4] *Institute of Railway Research, School of Computing and Engineering, University of Huddersfield, UK and ISEL, IPL, Lisboa, Portugal, j.pombo@hud.ac.uk*

ABSTRACT — *The contact between a wheel and a rail in the context of railway dynamics is mostly the result of the interaction of two convex surfaces. However, when negotiating sharp curves and due to worn profiles, the conformal contact tends to occur. In this type of interaction, the contact zone cannot be contained in a single plane as opposed to the non-conformal case. Hence, a new methodology to deal with conformal contact in the framework of railway dynamics is proposed in this work. A curved axis in the lateral direction is considered, and it is used to measure the separation between profiles. Moreover, the contact patch is divided into strips in which it is locally planar, and the pressure distribution is estimated based on Kik-Piotrowski model. The interaction between a wheel and rail has been tested for four static cases. The preliminary results show that this methodology can be a reliable alternative to the use of more computationally intensive approaches as the boundary or finite element methods.*

1 Introduction

The dynamic simulation of railway vehicles based on multibody methodologies is nowadays a reliable approach to prevent derailment, design components, study the vehicle performance for a certain railway network, among others [1]. In this context, the wheel-rail contact interaction is fundamental not only in the study of the vehicle dynamics, but also in the prediction of rolling contact fatigue or wear, profile optimization, just to mention a few [2]. For these purposes, the shape and size of the contact patch need to be properly determined, as well as the normal pressure and tangential tractions, including for the interaction cases in which conformal contact takes place.

The wheel-rail interaction stands as a particular case of contact modeling using multibody formulation, where one of the contacting bodies is rolling over the other. The resolution of contact problems is quite frequent in the context of a multibody system dynamics, and it comprises three fundamental steps [3]. First, the geometry of the interacting bodies must be defined, that is, the mathematical description of contacting surfaces, either by continuous functions or discrete points. Secondly, the contact detection between both bodies has to be performed to find the potential contact points. The degree of complexity of this task is intimately associated with the shape of the contacting surfaces. Finally, a proper contact model is utilized to evaluate the contact forces, either on the normal and tangential directions. Depending on the comprehensiveness of the contact model, it can consider a

single point of contact or a finite contact area, with an Hertzian or non-Hertzian pressure distribution. Any of these steps takes a fundamental role on the obtained dynamic response of the system, as well as in the computational efficiency of the multibody simulation.

In what concerns to the wheel-rail contact force models, two main approaches can be employed, often called constraint and elastic approaches. The first involves the definition of nonlinear kinematic constraints [4], which limits the number of degrees of freedom of the wheel with respect to the rail to five. In turn, the elastic approach does not constrain any degree of freedom because it allows the interpenetration between both surfaces. The constraint approach is often faster since it solves the contact detection and normal force evaluation simultaneously with the equations of motion, however, it provides a rigid contact and does not generate information about the contact patch and normal pressure distribution. Therefore, the elastic approach is more commonly found to represent the wheel-rail interaction [3,5-10]. Different strategies have been explored, from fast and approximate methods [3,5] to more complex and realistic models [6]. Naturally, the degree of complexity of the applied method is closely linked with the required computational cost which implies always a trade-off between accuracy and efficiency. Furthermore, these methodologies can be implemented with online or offline calculation, that is, respectively, the forces are calculated for each contact case or they are interpolated from pre-calculated tables. The offline calculation is of substantial interest to be utilized with computationally expensive methods, such as finite element method or boundary element method [6,10-12]. Most of the wheel-rail contact force models available in the literature are limited to their application in non-conformal contact cases. Although this covers most of the possible interaction scenarios, in which the rail interacts directly with the tread or flange, when negotiating sharp curves or due to worn profiles, the conformal contact tends to occur in the running profile fillet zone. Moreover, the study of conformal contact is not yet a very deepened topic, although some researchers have been paying attention to this issue in the last few years [10-13]. At this moment, there is no established standard model for the evaluation of the contact forces in a conformal situation under multibody simulations.

The main goal of this work is to propose a new methodology to deal with the evaluation of the normal contact force for the wheel-rail interaction in a conformal contact scenario. This approach considers rigid wheel and rail bodies, and utilizes their virtual penetration to evaluate the pressure distribution in the contact patch. Thus, this paper is organized as follows. Section 2 presents the issues to be taken into consideration when modelling conformal contact in contrast with a non-conformal one. Section 3 describes not only the determination of the surface separation function and, hence, the contact patch, but also the normal forces developed over the non-planar contact patch. In Section 4, some static cases of interaction between a wheel and rail profiles are utilized to demonstrate the effectiveness of this methodology. Finally, the main conclusions of this work are summarized in Section 5.

2 Conformal Contact Problem

Most of the wheel-rail contact theories relies on some simplified assumptions, such as that a single normal direction can be considered for the entire contact patch and the validity of the half-space approach [11]. Notwithstanding, these assumptions are often violated during the vehicle operation, namely when conformal contact occurs.

When two arbitrary convex bodies come into contact, assuming they are rigid, an interpenetration region would appear as represented in Fig. 1(a). However, considering the elasticity of the contacting bodies, their surfaces tend to deform and establish an effective contact area which is smaller than the interpenetration region. In this case, the contact patch is planar, which means that the normal pressure distribution would have the same direction over the entire contact zone. On the other hand, when a convex body and a concave body, come into contact as displayed in Fig. 1(b), under the assumption of rigid bodies, an interpenetration region also exists. In a similar manner, the effective contact zone is also smaller due to the elastic deformation of the surfaces. However, in the conformal case, the resulting contact patch has a curved shape as schematized in Fig. 1(b). Note

that the conformal contact is only possible if the radius of curvature of the convex surface is not bigger than the radius of the concave one.

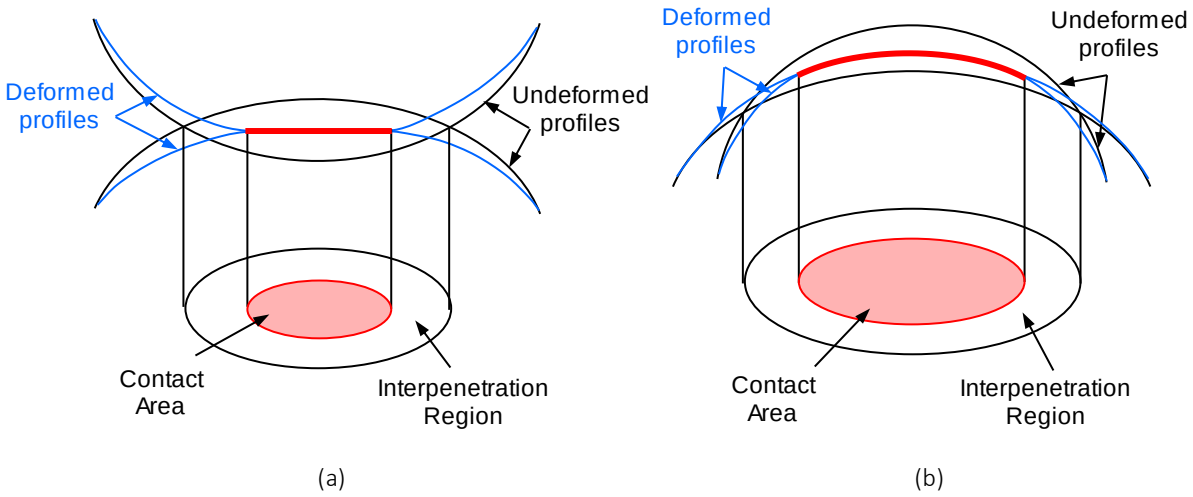

Fig. 1: Schematic representation of the contact region for (a) a non-conformal case (plane contact patch) and (b) conformal case (curved contact patch)

Thus, the main distinction on the conformal contact is that the contact patch is no longer flat, as in the non-conformal case. In the conformal contact, there is no plane where the contact patch can be projected and, therefore, the concept of global normal and tangential forces is not applied anymore. Moreover, in these conditions, the spin creepage is not constant through the contact region. Hence, the proposed methodology must consider a variation of the contact angle along the patch according to the profiles curvatures. The elastic half-space assumption can be kept since it is valid for smaller variations of the contact angle.

3 Methodology for Contact Resolution

In this section, a new methodology to evaluate the normal contact pressure in the wheel-rail interaction for conformal contact scenarios is presented. First, a complete description of the wheel and rail geometries is delivered, as well as their parametrization so the proposed model can be implemented. Secondly, the strategy for the determination of the curved contact patch is detailed. Then, the calculation of the normal contact force over the contact patch is demonstrated.

3.1 Wheel and Rail Parametrization

The forces generated during the wheel-rail interaction have a huge dependence on their geometries, therefore, it is of paramount importance to accurately define the contacting surfaces. Thus, the wheel and rail surfaces are parametrized, i.e., any point of their surfaces can be defined by two coordinates. Figure 2 shows how to obtain the coordinates of any point in the global coordinate system.

The surface of each rail is obtained through the sweep of its cross-section along a certain path which is described by a set of nodal points [14-15]. These nodal points define the position and orientation of the rail as function its arclength, s_r^{side}. The position of the origin of the rail profile is defined by $\mathbf{r}_r^{side}$, and its orientation is given by a set of vectors $\mathbf{t}_r^{side}$, $\mathbf{n}_r^{side}$ and $\mathbf{b}_r^{side}$ are, respectively, the tangent, normal and binormal vectors depicted in Fig. 2. Note that the superscript *side* can be defined as "L" or "R" when it refers to the left or right side, respectively. Moreover, the rail cross-section is defined through a set of nodal points defined in a local reference system $\left(u_r^{side} / f_r^{side}\right)$ as depicted in Fig. 3(a), where u_r^{side} is one of the surface parameters and f_r^{side} is the dependent coordinate. In turn, the wheel surface is described as a revolution of its cross-section about its axis. In

that sense, a point in the wheel surface is defined by the angular position s_{w}^{side}, and the lateral coordinate u_{w}^{side}. The wheel cross-section is defined in a local reference system $\left(u_{\mathrm{w}}^{side} / f_{\mathrm{w}}^{side}\right)$ in a similar manner to the rail as represented in Fig. 3(b). In order to define the wheel and rail profiles, cubic polynomials are generated to interpolate any point within the profiles domain [3].

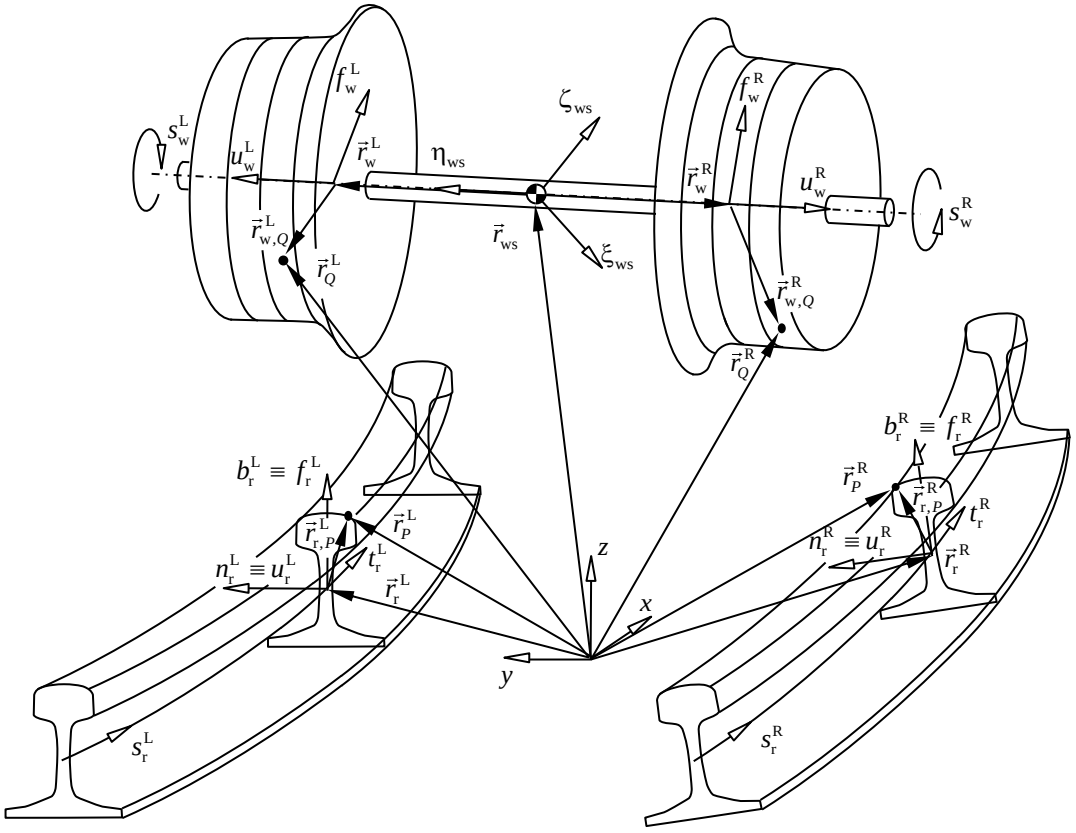

Fig. 2: Parametrization of wheel and rail surfaces

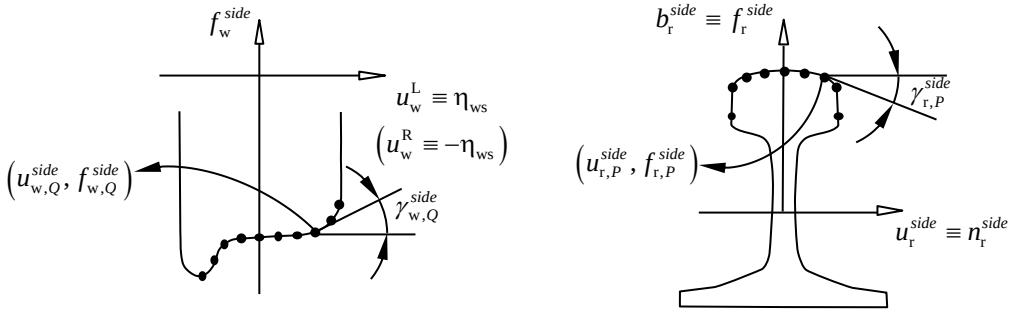

Fig. 3: Definition of (a) wheel and (b) rail profiles

The position of an arbitrary point Q in the wheel surface of a certain wheelset, as shown in Fig. 2, can be expressed as

$$\mathbf{r}_{Q}^{side} = \mathbf{r}_{\mathrm{ws}} + \mathbf{r}_{\mathrm{w}}^{side} + \mathbf{r}_{\mathrm{w},Q}^{side} \tag{1}$$

where $\mathbf{r}_{\mathrm{ws}}$ denotes the position vector of the wheelset center of mass, $\mathbf{r}_{\mathrm{w}}^{side}$ represents the distance between the wheelset center of mass and the wheel profile origin, and $\mathbf{r}_{\mathrm{w},Q}^{side}$ is the distance vector of the wheel profile origin and point Q. Thus, $\mathbf{r}_{\mathrm{w}}^{side}$ can be defined as

$$\mathbf{r}_{\mathrm{w}}^{\mathrm{L}} = \mathbf{A}_{\mathrm{ws}}\begin{bmatrix}0 & H/2 & 0\end{bmatrix}^{\mathrm{T}} \quad , \quad \mathbf{r}_{\mathrm{w}}^{\mathrm{R}} = \mathbf{A}_{\mathrm{ws}}\begin{bmatrix}0 & -H/2 & 0\end{bmatrix}^{\mathrm{T}} \tag{2}$$

in which $\mathbf{A}_{\mathrm{ws}}$ represents the transformation matrix of the wheelset, and H is the distance between both wheels profiles. Moreover, $\mathbf{r}_{\mathrm{w},Q}^{side}$ can be given as follows

$$\mathbf{r}_{\mathrm{w},Q}^{side} = \mathbf{A}_{\mathrm{ws}}\mathbf{A}_{\mathrm{w}}^{side}\begin{bmatrix}0 & u_{\mathrm{w},Q}^{side} & f_{\mathrm{w},Q}^{side}\end{bmatrix}^{\mathrm{T}} \tag{3}$$

where $u_{\mathrm{w},Q}^{side}$ and $f_{\mathrm{w},Q}^{side}$ are the coordinates of point Q in the local coordinate system represented in Fig. 3(a), and $\mathbf{A}_{\mathrm{w}}^{side}$ is the transformation matrix from this coordinate system to the wheelset reference frame, which can be defined as

$$\mathbf{A}_{\mathrm{w}}^{\mathrm{L}} = \begin{bmatrix}\cos\left(s_{\mathrm{w},Q}^{\mathrm{L}}\right) & 0 & \sin\left(s_{\mathrm{w},Q}^{\mathrm{L}}\right)\\ 0 & 1 & 0\\ -\sin\left(s_{\mathrm{w},Q}^{\mathrm{L}}\right) & 0 & \cos\left(s_{\mathrm{w},Q}^{\mathrm{L}}\right)\end{bmatrix} \quad , \quad \mathbf{A}_{\mathrm{w}}^{\mathrm{R}} = \begin{bmatrix}-\cos\left(s_{\mathrm{w},Q}^{\mathrm{R}}\right) & 0 & -\sin\left(s_{\mathrm{w},Q}^{\mathrm{R}}\right)\\ 0 & -1 & 0\\ -\sin\left(s_{\mathrm{w},Q}^{\mathrm{R}}\right) & 0 & \cos\left(s_{\mathrm{w},Q}^{\mathrm{R}}\right)\end{bmatrix} \tag{4}$$

This transformation matrix depends on the angular coordinate of point Q on the wheel surface. Thus, for the complete definition of a point in the wheel surface, only the parameters $u_{\mathrm{w},Q}^{side}$ and $s_{\mathrm{w},Q}^{side}$ are required.

Moreover, the normal vector to the wheel surface in point Q can be calculated as

$$\mathbf{n}_{\mathrm{w}}^{side} = \mathbf{A}_{\mathrm{ws}}\mathbf{A}_{\mathrm{w}}^{side}\begin{bmatrix}0 & \sin\left(\gamma_{\mathrm{w},Q}^{side}\right) & -\cos\left(\gamma_{\mathrm{w},Q}^{side}\right)\end{bmatrix}^{\mathrm{T}} \tag{5}$$

where $\gamma_{\mathrm{w},Q}^{side}$ is the angle shown in Fig. 3(a) that can be determined by

$$\gamma_{\mathrm{w},Q}^{side} = \tan^{-1}\left(\frac{\mathrm{d}f_{\mathrm{w}}^{side}\left(u_{\mathrm{w},Q}^{side}\right)}{\mathrm{d}u_{\mathrm{w}}^{side}}\right) \tag{6}$$

In what concerns to the definition of the position vector of an arbitrary point P in the rail surface, as displayed in Fig. 2, it can be expressed as

$$\mathbf{r}_{P}^{side} = \mathbf{r}_{\mathrm{r}}^{side} + \mathbf{r}_{\mathrm{r},P}^{side} \tag{7}$$

where $\mathbf{r}_{\mathrm{r}}^{side}$ denotes the position vector of the origin of the rail profile and depends on the rail arclength s_{r}^{side}, and $\mathbf{r}_{\mathrm{r},P}^{side}$ is the distance vector of the rail profile origin and point P given by

$$\mathbf{r}_{\mathrm{r},P}^{side} = \mathbf{A}_{\mathrm{r}}^{side}\begin{bmatrix}0 & u_{\mathrm{r},P}^{side} & f_{\mathrm{r},P}^{side}\end{bmatrix}^{\mathrm{T}} \tag{8}$$

where $u_{\mathrm{r},P}^{side}$ and $f_{\mathrm{r},P}^{side}$ are the coordinates of point P in the local two-dimensional coordinate system represented in Fig. 3(b), and $\mathbf{A}_{\mathrm{r}}^{side}$ is the transformation matrix for the orientation of the rail cross-section which can be described as

$$\mathbf{A}_{\mathrm{r}}^{side} = \begin{bmatrix}\mathbf{t}_{\mathrm{r}}^{side} & \mathbf{n}_{\mathrm{r}}^{side} & \mathbf{b}_{\mathrm{r}}^{side}\end{bmatrix} \tag{9}$$

Hence, an arbitrary point P can be characterized only by the two surface parameters $u_{\mathrm{r},P}^{side}$ and $s_{\mathrm{r},P}^{side}$. Analogously to the wheel, the normal vector to the rail surface in point P can be evaluated as

$$\mathbf{n}_{\mathrm{r}}^{side} = \mathbf{A}_{\mathrm{r}}^{side}\begin{bmatrix} 0 & -\sin\left(\gamma_{\mathrm{r},P}^{side}\right) & \cos\left(\gamma_{\mathrm{r},P}^{side}\right)\end{bmatrix}^{\mathrm{T}} \tag{10}$$

in which $\gamma_{\mathrm{r},P}^{side}$ is the angle displayed in Fig. 3(b), and can be estimated as

$$\gamma_{\mathrm{r},P}^{side} = \tan^{-1}\left(\frac{\mathrm{d}f_{\mathrm{r}}^{side}\left(u_{\mathrm{r},P}^{side}\right)}{\mathrm{d}u_{\mathrm{r}}^{side}}\right) \tag{11}$$

Since the contact between two conformal surfaces generates a curved contact patch, within the methodology proposed here, it is necessary to parametrize the cross-section as function of its arclength. Therefore, the arclength can be calculated as a function of the lateral coordinate of the profile, wheel or rail, using the already generated polynomials as

$$L_k(u_k) = \int_{u_0}^{u_k}\sqrt{1+\left(\frac{\mathrm{d}f_k(u_k)}{\mathrm{d}u_k}\right)^2}\,\mathrm{d}u_k \quad , \quad k = \mathrm{r},\mathrm{w} \tag{12}$$

where u_0 identifies the first nodal point of the cross-section. This parametrization does not depend on the side of the wheel or rail considering that both profiles have the same shape. Thus, it allows to obtain a position of certain point on the surface for a given arclength, since it can be utilized to calculate the lateral coordinate of the cross-section.

3.2 Contact Patch Parametrization

This formulation proposes a methodology for the calculation of the normal contact force in a conformal contact scenario being used an elastic approach based on Kik-Piotrowski model [8]. Therefore, the contact detection process is out of the scope of this work. In that sense, it is assumed that the maximum penetration point is known. Thus, $\mathbf{r}_Q$ and $\mathbf{r}_P$ are the wheel and rail contact points, respectively, which satisfy the contact conditions, as depicted in Fig. 4(a). For sake of simplicity, the superscripts "L" and "R" for the left and right sides, respectively, are disregarded, since the following formulation is not affected by the wheel and rail side.

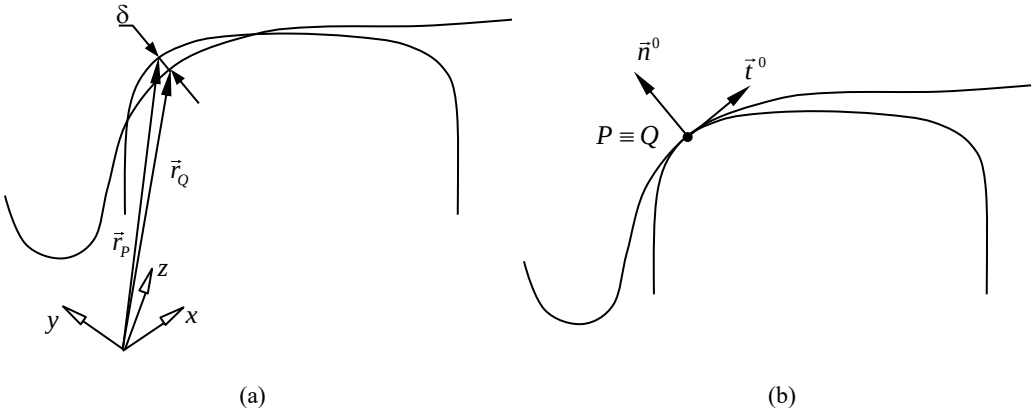

(a) (b)

Fig. 4: Representation of the profiles and contacting points (a) with and (b) without penetration

Since the main contact points of the two bodies are known, the penetration vector, which represents the distance between them, can be written as

$$\mathbf{d} = \mathbf{r}_Q - \mathbf{r}_P \tag{13}$$

Thus, the maximum penetration is calculated as

$$\delta = \sqrt{\mathbf{d}^{\mathrm{T}}\mathbf{d}} \tag{14}$$

Then, the separation between undeformed surfaces must be determined, that is, the distance between the wheel and rail surfaces without penetration or deformations. Consequently, the two profiles are moved away with the direction of the penetration vector, which makes them tangent in the contact point as shown in Fig. 4(b). Moreover, the normal direction vector in the contact point is calculated as

$$\mathbf{n}^0 = \frac{\mathbf{d}}{\delta} \tag{15}$$

and the tangent vector $\mathbf{t}^0$ is obtained through a rotation of 90º.

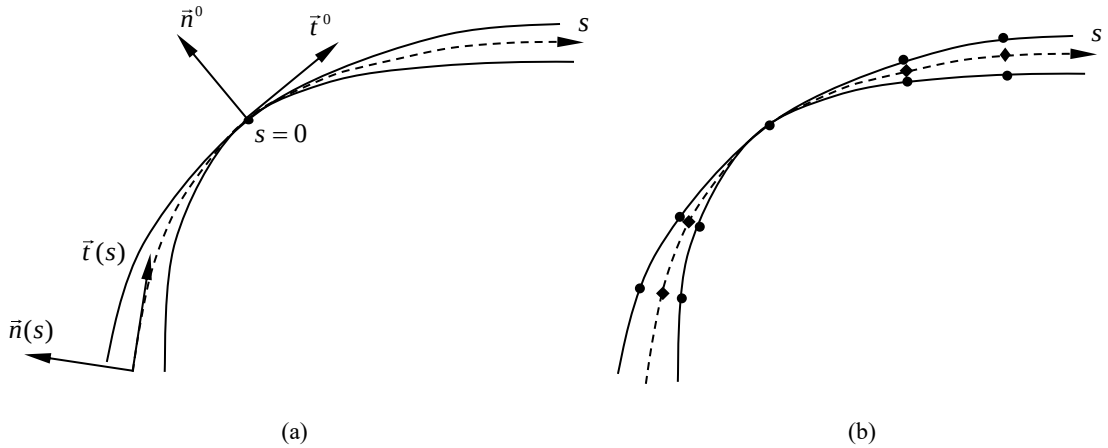

(a) (b)

Fig. 5: Representation of (a) the curved axis s along the contact patch and (b) profile points for each strip

As it was discussed in Section 2, the contact patch in conformal case is curved, which implies that the distance between both profiles cannot be measured in the same direction $\mathbf{n}_0$ for all the domain. Thus, it is fundamental to consider a variable normal direction along the contact patch. In this method, a curved axis s with origin in the main contact point, and defined between the wheel and rail profiles, is taken into consideration as depicted in Fig. 5(a). Assuming that, in the contact patch, the wheel and rail have constant curvature in the rolling direction x, the separation between profiles can be expressed as

$$n(x,s) = g(s) + \kappa^x x^2 \tag{16}$$

where $g(s)$ is the undeformed distance function between the two profiles along the direction s, and κ^x is the combined curvature in the rolling direction given by

$$\kappa^x = \frac{1}{2}\left(\frac{1}{R_{\mathrm{r}}^x} + \frac{1}{R_{\mathrm{w}}^x}\right) \tag{17}$$

in which the R_{r}^x and R_{w}^x are the radii of curvature of wheel and rail surfaces in the rolling direction, respectively. Assuming that the rail is flat, both radii can be calculated as

$$R_{\mathrm{r}}^x \approx \infty \Rightarrow \kappa_{\mathrm{r}}^x = 0 \tag{18}$$

$$R_{\mathrm{w}}^{x}=\left|f_{\mathrm{w}}\left(u_{\mathrm{w}}\right)\right|\sqrt{1+\left(\frac{\mathrm{d}f_{\mathrm{w}}\left(u_{\mathrm{w}}\right)}{\mathrm{d}u_{\mathrm{w}}}\right)^{2}} \tag{19}$$

Thus, substituting Eqs. (17-19) into Eq. (16), it can be rewritten in the following form

$$n\left(x,s\right)=g\left(s\right)+\frac{x^{2}}{2R_{\mathrm{w}}^{x}} \tag{20}$$

Hence, the underformed distance function $g(s)$ has to be estimated. For that purpose, the contact patch is divided into strips along s direction, and the patch is assumed to be locally planar inside the domain of each strip. The more refined the contact patch, the greater the resemblance with a perfectly curved patch. Since the contacting points in both surfaces are known, the respective lateral coordinates of both surfaces can be obtained, u_{r}^{0} and u_{w}^{0}, in which the superscript "0" denotes the origin of s axis. Then, the arclength position in the profiles can be derived with the previous parametrization, providing L_{r}^{0} and L_{w}^{0}. Thus, the points of the remining strips are obtained through the variation of the position in the arclength of the both profiles as follows

$$L_{k}^{i}=L_{k}^{0}+\Delta s\cdot i\quad,\quad k=\mathrm{r},\mathrm{w} \tag{21}$$

where Δs is the width of each strip, and i refers to the index of the strip which is positive or negative according to the s axis. Then, the corresponding parameters u_{r}^{i} and u_{w}^{i} can be determined for each strip, which allows the calculation of the position vector of the points in both profiles represented by circles in Fig. 5(b). These points can be used to determine the undeformed distance function in each strip as

$$g\left(s\right)=\begin{cases}\dfrac{\left(\mathbf{r}_{\mathrm{w}}^{i}-\mathbf{r}_{\mathrm{r}}^{i}\right)\cdot\left(\mathbf{n}_{\mathrm{r}}^{i}-\mathbf{n}_{\mathrm{w}}^{i}\right)}{\left\|\mathbf{n}_{\mathrm{r}}^{i}-\mathbf{n}_{\mathrm{w}}^{i}\right\|} & \text{if } s\neq 0\\ 0 & \text{if } s=0\end{cases} \tag{22}$$

where the $\mathbf{n}_{\mathrm{w}}^{i}$ and $\mathbf{n}_{\mathrm{r}}^{i}$ are the normal vectors to the wheel and rail surfaces for the arclength L_{r}^{i} and L_{w}^{i}, respectively, and can be calculated recurring to Eq. (5) and Eq. (10).

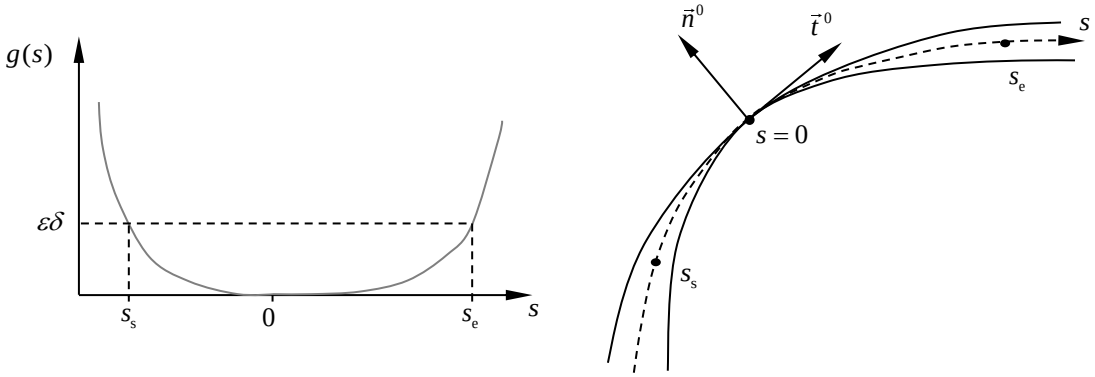

(a) (b)

Fig. 6: (a) Generic representation of the undeformed distance function, and
(b) respective illustration of the start and end of the contact patch

Generally, the obtained undeformed distance function presents an aspect similar to Fig. 6(a). Thus, to estimate the size of the contact patch along s axis, it is considered the region where the underfomed distance

function is lower than the maximum penetration. However, if the surfaces deformation is taken into account, the contact patch must be estimated using a smaller virtual penetration as

$$\delta_0 = \varepsilon\delta \tag{23}$$

where ε is a constant value set to 0.55 [8]. Therefore, the contact patch boundaries are determined by the intersection between a horizontal line equal to the virtual penetration and the undeformed distance function, as depicted in Fig. 6(a). The respective representation of the start point, s_s, and end point, s_e, of the contact is provided in Fig. 6(b). Furthermore, the interpenetration function of the profiles is defined by

$$h(s) = \begin{cases} \delta_0 - g(s) & \text{if } g(s) \le \delta_0 \\ 0 & \text{if } g(s) > \delta_0 \end{cases} \tag{24}$$

which allows the calculation of the length of each strip using Eq. (16), therefore, *x*-coordinate of the leading edge of a given strip is determined as

$$x_L(s) = \sqrt{2R_w^x h(s)} \tag{25}$$

Moreover, to fully describe the contact patch, it is of paramount importance to specify the orientation of each strip. Bearing that in mind, the position of the strips points along the *s* axis, represented by squares in Fig. 5(b), must be calculated. Hence, it is defined as the medium point of the wheel and rail profile points for a given strip *i*, being expressed as

$$\mathbf{r}_s^i = \frac{\mathbf{r}_r^i + \mathbf{r}_w^i}{2} \tag{26}$$

Thus, the tangential vector for each strip can be approximated by

$$\mathbf{t}(s) = \begin{cases} \dfrac{\mathbf{r}_s^{i+1} - \mathbf{r}_s^i}{\left\|\mathbf{r}_s^{i+1} - \mathbf{r}_s^i\right\|} & \text{if } s = s_s \\ \dfrac{\mathbf{r}_s^i - \mathbf{r}_s^{i-1}}{\left\|\mathbf{r}_s^i - \mathbf{r}_s^{i-1}\right\|} & \text{if } s = s_e \\ \dfrac{\mathbf{r}_s^{i+1} - \mathbf{r}_s^{i-1}}{\left\|\mathbf{r}_s^{i+1} - \mathbf{r}_s^{i-1}\right\|} & \text{otherwise} \end{cases} \tag{27}$$

and the normal vector for each strip $\mathbf{n}(s)$ is obtained through the rotation of the tangent vector by 90º.

3.3 Contact Force Evaluation

In what concerns to the normal pressure distribution, an approach based on Kik-Piotrowski model [8] is proposed here. Thus, since it assumed a constant curvature in the rolling direction, the contact presents Hertzian properties in that direction which leads to a semi-elliptical distribution of the normal pressure. In turn, in the transverse direction, it is proportional to the interpenetration between profiles. Hence, the normal pressure distribution inside the contact patch is written as

$$p(x,s) = \frac{p_0}{x_L(0)}\sqrt{x_L^2(s) - x^2} \tag{28}$$

where p_0 is the maximum pressure. Since the displacement on the main contact point is known, and making use of the Boussinesq's influence function to describe the pressure-displacement relationship [8], the maximum pressure is calculated as

$$p_0 = \frac{\pi E \delta}{2\left(1-\sigma^2\right)} x_{\mathrm{L}}(0)\left(\int_{s_{\mathrm{s}}}^{s_{\mathrm{e}}}\int_{-x_{\mathrm{L}}}^{x_{\mathrm{L}}} \frac{\sqrt{{x_{\mathrm{L}}}^2(s)-x^2}}{\sqrt{x^2+s^2}}\,\mathrm{d}x\mathrm{d}s\right)^{-1} \tag{29}$$

in which E represents the Young's modulus, and σ refers to the Poisson ratio. Note that, in the previous equation, the integral part is a divergent improper integral, which means that its numerical resolution requires special care.

Generally, to obtain the total normal contact force, the pressure distribution is integrated over the contact patch. However, in this case, since each strip is locally planar and has a different normal direction, the normal pressure must be integrated separately for each strip. Thus, the magnitude of the normal force for a single strip is determined as

$$N_i = \frac{p_0}{x_{\mathrm{L}}(0)}\int_{-x_{\mathrm{L}}}^{x_{\mathrm{L}}} \sqrt{{x_{\mathrm{L}}}^2(s)-x^2}\,\mathrm{d}x\Delta s \tag{30}$$

Finally, the total force due to the normal pressure can be calculated through the vector sum of the contribution of each strip, and it can be written in following form

$$\mathbf{N} = \sum_{i=1}^{N_{\mathrm{S}}} N_i \mathbf{n}_i \tag{31}$$

where N_{S} is the total number of contacting strips.

4 Example of Application

In this section, a static case of interaction between a wheel and a rail is utilized as an example of application to demonstrate the effectiveness of this methodology. For that purpose, the light rail vehicle wheel profile and a UIC54 rail [16], whose cross-sections as are displayed in Fig. 7, are here utilized. The remaining geometric and material properties necessary to the contact model are listed in Tab. 1.

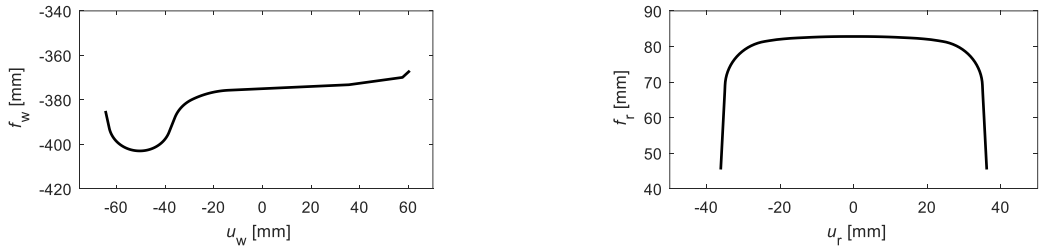

(a) (b)

Fig. 7: (a) Wheel and (b) rail profiles

Parameter	Value
Wheel Nominal Radius, R	375 mm
Nominal Distance between Wheels Profiles, H	1055 mm
Rail Cant	1/20
Young's Modulus, E	208 GPa
Poisson Ratio, σ	0.3

Tab. 1: Geometric and material properties utilized in the simulation

Although the proposed methodology permits the calculation of the contact force for a given penetration of the profiles, in these static analyses, the contact patch and normal pressure distribution are calculated for a specified vertical force. Therefore, for a fixed lateral displacement, the vertical position of the wheelset is iteratively determined using Newton-Raphson method to ensure that the imposed vertical load is 24000 N. Different contact cases are tested by displacing the wheel over the rail in the lateral direction as depicted in Fig. 8, namely $\Delta y = 0$, 8, 9 and 10 mm. Although a null displacement represents the nominal position of the wheelset, in which the contact interaction is non-conformal, the proposed methodology is also applied. In the remaining cases, the contact occurs in the transition between the tread and flange, therefore, it results from the interaction between conformal surfaces.

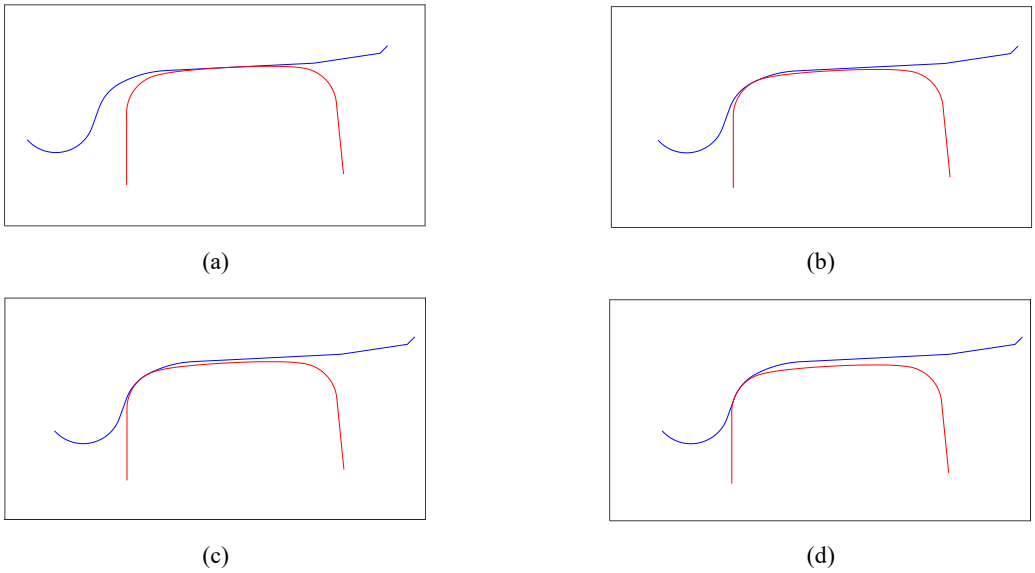

(a) (b) (c) (d)

Fig. 8: Wheel-rail contact interaction for different lateral displacements:
(a) $\Delta y = 0$ mm; (b) $\Delta y = 8$ mm; (c) $\Delta y = 9$ mm; and (d) $\Delta y = 10$ mm

The contact patch was determined for the four contact scenarios, and the results are displayed in Fig. 9 in which the s axis is projected. Moreover, the number of contacting strips, the maximum normal pressure in the contact patch and the variation of the contact angle are listed in Tab. 2. For the first case ($\Delta y = 0$ mm), the patch assumes an almost elliptical shape as expected (see Fig. 9(a)). The obtained contact zone is nearly planar, with a variation of the contact angle of only 0.63º, which meets the assumptions of the non-conformal contact. In what concerns to the conformal contact cases, the patches show a more elongated shape due to the lower local curvature of the wheel in the rolling direction. Hence, to the same vertical load, the number of contacting strips is reduced. In turn, the maximum pressure increases to balance the higher inclination of the contact patch which reduces its contribution to the vertical load.

Regarding the variation of the contact angle, the three conformal scenarios have a meaningful variation of the contact angle when compared to the planar case, which has a significant impact in the resultant contact force calculation. However, since the maximum variation is 13.2º, which occurs for a lateral displacement of 9 mm, the half-space assumption can be held without introducing substantial inaccuracy.

	$\Delta y = 0$	$\Delta y = 8$	$\Delta y = 9$	$\Delta y = 10$
Number of Strips, N_S	93	23	37	25
Maximum pressure, p_0 [Pa]	6.14×10^8	2.04×10^9	1.42×10^9	2.78×10^9

Variation of the contact angle [º]	0.63	6.51	13.2	10.3

Tab. 2: Results for the number of strips, maximum pressure and variation of the contact angle for the different tested cases

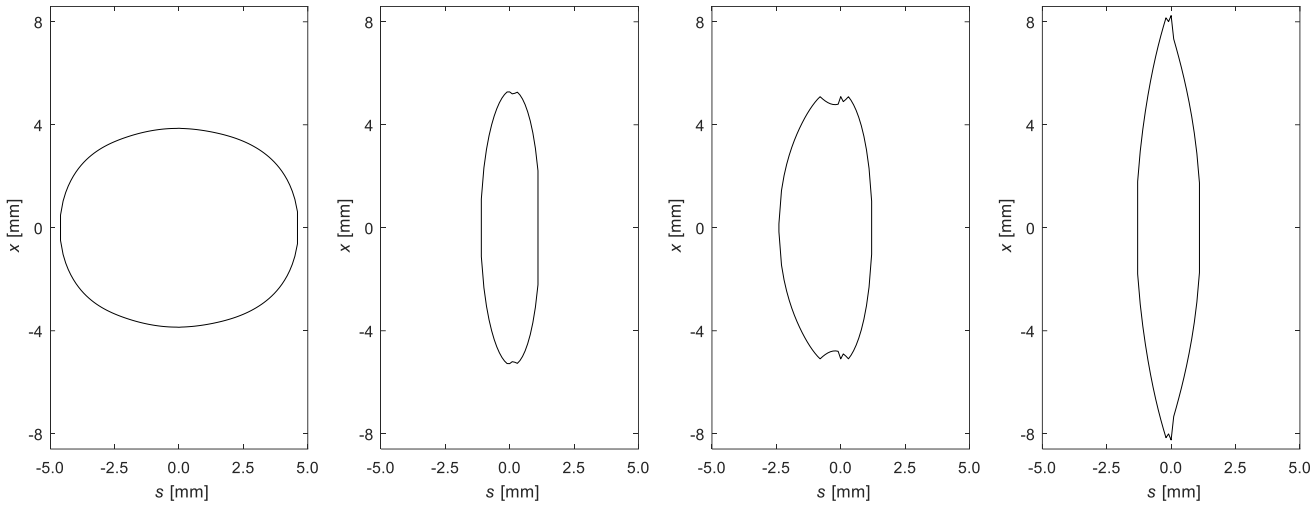

(a) (b) (c) (d)

Fig. 9: Contact patch for the different tested cases:
(a) $\Delta y = 0$ mm; (b) $\Delta y = 8$ mm; (c) $\Delta y = 9$ mm; and (d) $\Delta y = 10$ mm

5 Conclusions

A new simplified approach to deal with conformal contact in the context of the wheel-rail interaction is presented in this paper. Most of the existing wheel-rail contact force models are limited to the interaction between convex surfaces, therefore, little attention has been paid to the conformal contact in which the contact patch cannot be contained in a single plane. Hence, the normal pressure over this area does not act in the same direction, and the concept of a global normal direction to the contact is not valid anymore. Bearing that in mind, this work proposes a new strategy to estimate the contact patch by measuring the profiles separation distance along a curved axis. Moreover, the contact zone is divided into strips in the lateral direction, in which the contact is locally planar, and an elliptical pressure distribution is considered inside each strip [8].

Preliminary results of the static interaction between a wheel and a rail profiles at four different configurations are also delivered using the proposed methodology. These results show that this method is able to take into account the variation of the contact angle through the patch, although this angle is sufficiently small to keep the elastic half-space assumption. Furthermore, it is necessary to compare the obtained results with more computationally expensive methods in order to have a proper validation of the presented approach. The contact detection strategy is not within the scope of this work, although the estimation of the main point of contact has a critical influence in the results of this method.

As future work, the implementation of this methodology in a multibody dynamics code must be accomplished. Moreover, one of the major drawbacks of this methodology relies on the fact that it does not account with the yaw effect to determine the contact patch, which might be a future development.

Acknowledgements

The first and second authors are supported by the Portuguese Foundation for Science and Technology (FCT) under grant PD/BD/114154/2016, MIT Portugal Program, and SFRH/BD/96695/2013, respectively. This work

has been supported by the FCT with the reference project UID/EEA/04436/2013, by FEDER funds through the COMPETE 2020 - Programa Operacional Competitividade e Internacionalização (POCI) with the reference project POCI-01-0145-FEDER-006941.

References

[1] N. Wilson, R. Fries, M. Witte, A. Haigermoser, M. Wrang, J. Evans, and A. Orlova, "Assessment of safety against derailment using simulation and vehicle acceptance tests: a worldwide comparison of state-of-the-art assessment methods," *Vehicle System Dynamics*, vol. 49, no. 7, pp. 1113-1157, 2011.

[2] S.Z. Meymand, A. Keylin, and M. Ahmadian, "A survey of wheel–rail contact models for rail vehicles," *Vehicle System Dynamics*, vol. 54, no. 3, pp. 386-428, 2016.

[3] J. Pombo, J. Ambrósio, and M. Silva, "A new wheel–rail contact model for railway dynamics," *Vehicle System Dynamics*, vol. 45, no. 2, pp. 165-189, 2007.

[4] A.A. Shabana, M. Tobaa, H. Sugiyama, and K.E. Zaazaa, "On the Computer Formulations of the Wheel/Rail Contact Problem," *Nonlinear Dynamics*, vol. 40, pp. 169-193, 2005.

[5] J.J. Kalker, "A fast algorithm for the simplified theory of rolling contact," *Vehicle System Dynamics*, vol. 11, no. 1, pp. 1-13, 1982.

[6] J.J. Kalker, *Three-Dimensional Elastic Bodies in Rolling Contact*. The Netherlands: Kluwer Academic Publishers, 1990.

[7] W. Kik, and J. Piotrowski, "A fast, approximate method to calculate normal load at contact between wheel and rail and creep forces during rolling," in: I. Zabory (Ed.) *Proceedings of 2nd Mini Conference on Contact Mechanics and Wear of Rail/Wheel System*, pp. 52-61, TU Budapest, Hungary, 1996.

[8] J. Piotrowski, and W. Kik, "A simplified model of wheel/rail contact mechanics for non-Hertzian problems and its application in rail vehicle dynamic simulations," *Vehicle System Dynamics*; vol. 46, no. 1,2, pp. 27-48, 2008.

[9] M.S. Sichani, R. Enblom, and M. Berg, "A novel method to model wheel-rail normal contact in vehicle dynamic simulation," *Vehicle System Dynamics*, vol. 52, no. 12, pp. 1752-1764, 2014.

[10] B. Liu, S. Bruni, and E. Vollebregt, "A non-Hertzian method for solving wheel–rail normal contact problem taking into account the effect of yaw," *Vehicle System Dynamics*, vol. 54, no. 9, pp. 1226-1246, 2016.

[11] E. Vollebregt, and G. Segal, "Solving conformal wheel–rail rolling contact problems," *Vehicle System Dynamics*, vol. 52, pp. 455-468, 2014.

[12] J. Blanco-Lorenzo, J. Santamaria, E.G. Vadillo, and N. Correa, "On the influence of conformity on wheel-rail rolling contact mechanics," *Tribology International*, vol. 103, pp. 647-667, 2016.

[13] J.-P. Pascal, and B. Soua, "Solving conformal contacts using multi-Hertzian techniques," *Vehicle System Dynamics*, vol. 54, no. 6, pp. 784-813, 2016.

[14] J. Pombo, and J. Ambrósio, "An Alternative Method to Include Track Irregularities in Railway Vehicle Dynamic Analyses," *Nonlinear Dynamics*, vol. 68, no. 1-2, pp. 161-176, 2012.

[15] J. Ambrósio, P. Antunes, and J. Pombo, "On the requirements of interpolating polynomials for path motion constraints," In: A. Kecskeméthy, and F., Geu Flores (eds) *Interdisciplinary Applications of Kinematics. Mechanisms and Machine Science*, vol. 26, pp. 179-197, 2015.

[16] H. Magalhães, J. Ambrósio, and J. Pombo, “Railway vehicle modelling for the vehicle–track interaction compatibility analysis,” *Proceedings of the Institution of Mechanical Engineers, Part K: Journal of Multi-body Dynamics*, vol. 230, no. 3, pp. 251-267, 2016.